

FORSCHUNGSZENTRUM
ROSSENDORF e.V.

FZR

Archiv-Ex.:

FZR-59

Oktober 1994

Preprint

S. Frauendorf, J. Meng and J. Reif

Tilted Cranking

To be published in proceedings of the
"Conference on Physics From Large γ -Ray Detector Arrays",
August 2-6, 1994, Berkeley, USA
Invited Lectures

Forschungszentrum Rossendorf e.V.
Postfach 51 01 19 · D-01314 Dresden
Bundesrepublik Deutschland
Telefon (0351) 591 3261
Telefax (0351) 591 3700
E-Mail frauendorf@gamma.fz-rossendorf.de

Tilted Cranking

S. Frauendorf, J. Meng and J. Reif

Institut für Kern- und Hadronenphysik, Forschungszentrum Rossendorf e.V.
PF 510119, 01314 Dresden, Germany

October 8, 1994

Abstract: The Tilted Axis Cranking theory is used to describe the coexistence of high and low K bands in yrast spectra of well deformed nuclei, magnetic rotation of transitional nuclei and to calculate the parameters of a rotational hamiltonian with a fourfold symmetry axis that generates $\Delta I = 4$ staggering in the yrast band

The orientation of the deformed density distribution relative to the (space fixed) angular momentum vector becomes a useful concept at high spin. Tilted Axis Cranking (TAC) [1] is the version of the meanfield theory that permits to calculate the the orientation of the deformed field together with the parameters that define its shape. Since its introduction [2] it has turned out to be a reliable approximation to calculate both energies and intra band transition probabilities. The possibility to construct classical vector diagrams showing the angular momentum composition is of great help to understand the structure of the rotational bands. In this talk I shall discuss three applications of TAC: i) multiband spektra containing high and low K bands, ii) shears bands and magnetic rotation and iii) an attempt to find the microscopic origin of $\Delta I = 4$ staggering.

1 Multiband spectra

In TAC one seeks HF solutions that rotate uniformly about the angular momentum axis \vec{J} that has a tilt with the symmetry axis of the deformed field. In order to find the angle ϑ one diagonalizes the single particle routhian

$$h' = h_{def} - \omega(\sin \vartheta j_1 + \cos \vartheta j_3) \quad (1)$$

where h_{def} is the hamiltonian of the non rotating deformed field, containing pairing if necessary. Each configuration constructed from the single particle or quasiparticle levels corresponds to a rotational band. Each band has its individual tilt that is determined by minimizing the total routhian $E'(\omega, \vartheta)$ at fixed ω . At the minimum the angular momentum vector and the angular velocity

$$\vec{J} = \langle \vec{j} \rangle \quad \vec{\omega} = (\omega \sin \vartheta, \omega \cos \vartheta) \quad (2)$$

are parallel [1]. As in the traditional cranking theory, which assumes that that axis of rotation coincides with one of the principal axes of the deformed field (Principal Axis Cranking - PAC), there exist several possibilities to calculate E' from the single particle

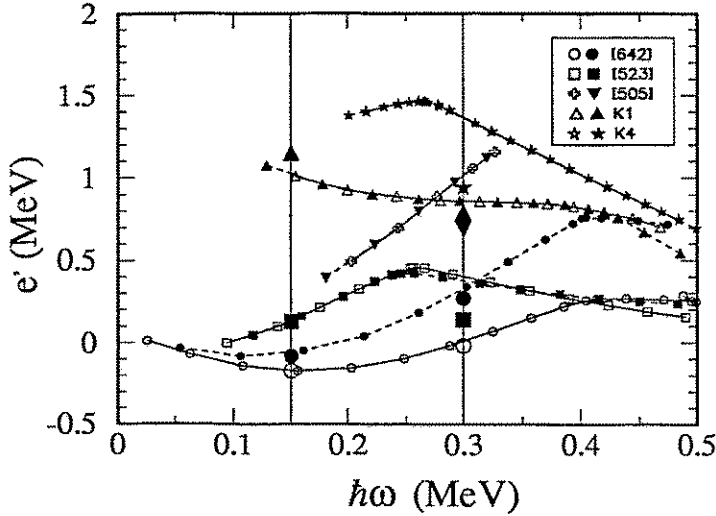


Figure 1: Experimental routhians of ^{163}Er compared to TAC calculations. The TAC routhians $E'(\omega)$ are shown as the large symbols on the two vertical lines located at the frequencies for which calculations have been carried out. The data is from [3]

wavefunctions generated by (1), as e. g. Strutinsky renormalization or Skyrme HF. So far, most calculations have been carried out in the HFB frame defined by the Pairing + QQ Interaction [1, 4]. If one is not interested in deformation changes it is sufficient to minimize $E' = \langle h' \rangle$.

The results of the TAC calculations are interpreted in the following way:

If $E'(\omega, \vartheta)$ has its minimum at $\vartheta = 0$ the band has not started yet. These solutions are disregarded. For each band there is a band head frequency (and spin as well) where the curvature of $E'(\omega, \vartheta)$ changes sign and the minimum begins to move towards 90° . The band head frequency and spin are characteristic for each band and experimentally well known.

Each TAC configuration represents a $\Delta I = 1$ band (i. e. two degenerate signatures) as long as $\vartheta < 90^\circ$. When $\vartheta = 90^\circ$ one has the ordinary PAC solution that is interpreted as a $\Delta I = 2$ band of the calculated signature. This change of interpretation leads to a discontinuous description (what is a well known consequence of symmetry breaking). However, there are no missing or extra states among the lowest bands. The only unphysical feature is a jump of the unfavored signature branch instead of a continuous onset of signature splitting.

Using the constraint $J = |\bar{J}| = I + 1/2$ one can fix the frequency ω and calculate the energy $E = E' + \omega J$. Often it is more convenient to introduce experimental routhians by means of the relations

$$\omega(I - \frac{1}{2}) = \frac{1}{2} (E(I) - E(I - 2)) \quad (3)$$

$$E'(I - \frac{1}{2}) = \frac{1}{2} (E(I) + E(I - 2)) - \omega(I - \frac{1}{2})(I - \frac{1}{2}) \quad (4)$$

The functions $I(\omega) - \frac{1}{2}$ and $E'(\omega)$, obtained in this way, can directly be compared with the calculated quantities $J(\omega)$ and $E'(\omega)$. This has the advantage that one can choose how accurately one wants to study the ω - dependence. Fig. 1 gives an example. TAC calculations only are carried out for $\omega = 0.15$ and 0.30 MeV . Ideally the calculated routhians

should lie at the intersections of the vertical lines with the experimental routhians. As seen, there is reasonable correspondence. In particular, the relative position of the high and low K bands is well accounted for. For the two bands denoted by K1 and K4 no TAC solution is found at $\omega = 0.15MeV$. Accordingly they start above this frequency in experiment. Note, eq.(3) differs from the definition of the frequency, usually used in CSM (which corresponds to ω_1). Since no assumption about J_3 ($=K$ at the band head in CSM) is involved, it is free of any ambiguity.

The intraband transition probabilities are calculated by means of the semiclassical expressions

$$BM1 = \frac{3}{8\pi} [\sin \vartheta (J_{3\pi} + 2.91S_{3\pi} - 2.61S_{3\nu}) - \cos \vartheta (J_{1\pi} + 2.91S_{1\pi} - 2.61S_{1\nu})]^2 \quad (5)$$

$$BE2 = \frac{15}{32\pi} [(\sin \vartheta)^2 eQ_0]^2 \quad (6)$$

where the vectors of angular momentum, \vec{J} , and of spin, $\vec{S} = \langle \vec{s} \rangle$ and the proton quadrupole moment, $Q_0 = \langle q_0 \rangle$ are calculated from the TAC conf. |). The free spin magnetic moments are attenuated by a factor of 0.7. Examples of calculations of transition probabilities can be found in refs. [1, 3, 4, 5].

In order to test the reliability of the TAC approximation we have carried out extensive comparisons of Two Particle + Rotor calculations with the TAC approximation to this model. Typically it is found that TAC describes rather well both the energies and the intra band transition probabilities of at least the lowest 5 bands. The agreement deteriorates with the excitation energy. It turns out that for high K bands only TAC gives a reliable description, whereas the procedures based PAC become problematic. The version that keeps J_3 constant equal to the K value at the band head becomes inaccurate for high spin, since even small changes of J_3 lead to substantial changes of the energies and transition probabilities. The other procedure that uses $J_3 = \sqrt{\langle j_3^2 \rangle}$ fails if more than one quasiparticle contribute to the total value of J_3 . For example, if the proton and the neutron both have the same k then one has a $K = 0$ and a $K = 2k$ band, whereas the PAC prescription results in two bands with $K = \sqrt{2}k$.

2 Magnetic Rotation

The recently discovered shears bands in the nuclei around ^{200}Pb (c. f. e. g. [4] and the lecture by H. Hübel) represent a new kind of rotation, whose nature was first understood in the framework of the TAC [1]. The experimental evidence is the observation of regular sequences of magnetic dipole transitions in the irregular spectra that are characteristic for spherical nuclei. The BM1 values are very large (several μ_N^2). If seen at all, the crossover transitions have very small BE2 values ($Q_t < 1(eb)^2$). Thus, one observes very regular bands with a substantial dynamic moment of inertia ($\mathcal{J}^{(2)} \sim 15...25MeV^{-1}$) in nuclei that are almost spherical.

The explanation of this apparent paradox is the shears mechanism that is illustrated in fig. 2. The active high j orbitals are $i_{13/2}$ and $h_{9/2}$ protons and $i_{13/2}$ neutron holes. The nucleus has a slight oblate deformation ($\epsilon_2 \sim -0.1$). This deformed field tends to align the protons with the symmetry axis 3 and the neutron holes with the 1 - axis, since the former have toroidal the latter dumbbell like density distributions. The bands start with \vec{j}_ν perpendicular to \vec{j}_π . Along the band angular momentum and energy increase by

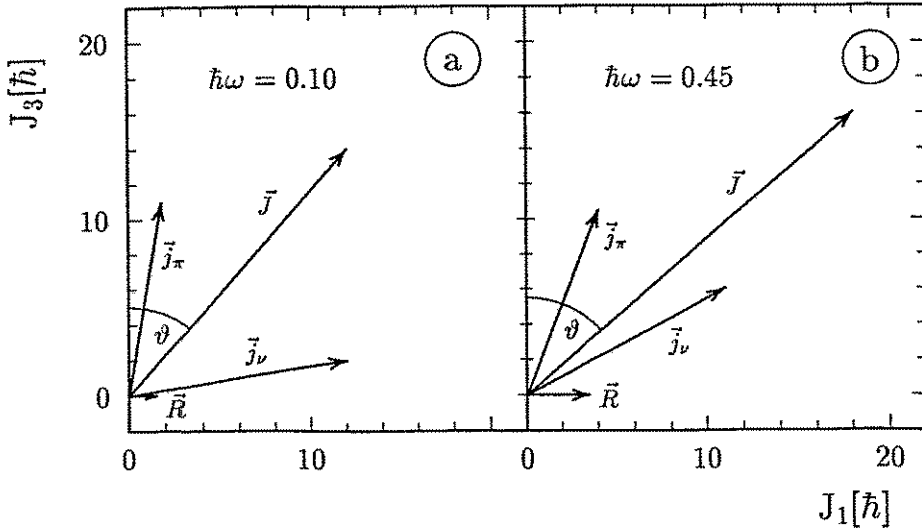


Figure 2: Angular momentum composition of the shears band $\pi h_{9/2}, \pi i_{13/2}, \pi [s_{1/2}]^{-2}, [\nu i_{13/2}]^{-2}$ in $^{198,200}\text{Pb}$ (from [4])

simultaneous alignment of both vectors with the total angular momentum \vec{J} , which keeps an angle of about 45° with the symmetry axis. The name "shears bands" alludes to the similarity with closing a pair of shears for sheep (which has a spring to keep it open).

Calculations based on the Pairing + QQ version of TAC account well for the energies and spins of the shears bands observed in $^{197-201}\text{Pb}$ [1, 4]. It turns out that most of the dynamic moment of inertia results from the shears mechanism, the part due to the deformation is about 7MeV^{-1} . The very small BE2 values are also well reproduced. TAC predicts BM1 values in the order of $5\mu_N^2$, which decrease with angular momentum. The decrease is a direct consequence of the shears mechanism, since closing the blades reduces the length of the component of the magnetic dipole moment perpendicular to \vec{J} . The M1 lifetime measurements are discussed in the lectures by H. Hübel [6] and R. Clark [7]. Some of the experimental BM1 values show the decrease with spin but some not. It seems to be important to clarify whether there exists a systematic discrepancy between theory and experiment.

States that are related to each other by recoupling of high j orbitals are quite common in nuclei with small deformation. They are also connected by fast M1 transitions. However, they do not show the regular level spacings over many spin values that justify the name band. In order to find the relation between these "multiplets" and the shears bands, we have studied the origin of the regular spacing by means of the spherical shell model. In order to keep to computational effort within reasonable limits we study the following model: The configuration space for neutrons is $[i_{13/2}]^{-n}$, $n = 1, 2$ and $[p_{1/2}, p_{3/2}, f_{5/2}]^n$, $n = 0, \dots, 12$. For the protons we assume the stretched configuration $[h_{9/2}i_{13/2}]_{J=11}$ combined with $[s_{1/2}]^{-2}$. We use experimental spherical single particle levels and a surface δ -interaction, whose strength is adjusted to the spherical spectra of the region. Effective charges and g -factors typical for the region are used. The physics of this model amounts to freeze the proton blade of the shears but to let the neutrons do what they like.

The calculations reproduce fairly well the energies and transition probabilities of the

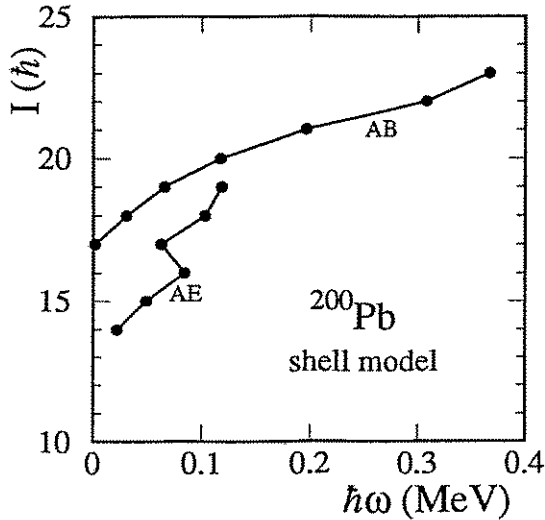


Figure 3: Angular momentum as function of the frequency (transition energy) calculated by means of the shell model. The bands AB and AE have the configurations $\pi[h_{9/2}, i_{13/2}]_{11}, \pi[s_{1/2}]^{-2}$ and $[\nu i_{13/2}]^{-2}, \nu[fp]^6$ and $\nu[i_{13/2}]^{-1}, \nu[fp]^7$, respectively.

observed shears bands. The BM1 values show the characteristic decrease with spin. Fig. 3 shows as an example the function $I(\omega)$ for two configurations in ^{200}Pb , where AB contains two and AE only one $\nu i_{13/2}$ holes. It illustrates the general tendency that the more high j -orbitals are forming the blade the more regular the band becomes. This holds also for the different proton configurations, which we have studied as well.

A second feature is illustrated by fig. 4 that summarizes the results for two $i_{13/2}$ neutron holes and different even numbers of neutrons in the fp states. There is a general increase of the energy with the angular momentum. This is a consequence of the short range interaction, which prefers a perpendicular orientation of the angular momentum vectors of the protons and neutron holes, because their spatial density distributions are tori or dumbbells, respectively. The level spacings are irregular if the fp shell is empty or full. The wavefunctions show that this irregularity is accompanied by changes of the orientation of the two $i_{13/2}$ neutron holes relative to each other. Regular bands appear only in the middle of the fp shell, where the wavefunctions show that the two $i_{13/2}$ neutron holes are predominantly coupled to $J = 12$. There is a gradual transition from the multiplets to the shears bands. Hence, the fp neutrons act as a kind of glue that keeps the two neutron holes in stretched coupling. Such a long stiff neutron blade can take on many different orientations with respect to the proton blade, resulting in a regular shears band.

How does the glue act? The wave function of the fp neutrons is mainly composed of states with $J = 0, 2, 4$, which may combine to a slightly deformed density distribution. The following feedback mechanism seems to be active:

On the one hand, the slightly deformed fp density aligns the orbitals forming a blade, on the other hand, the spatial density distributions of these orbitals induce the deformation of the fp density.

Regular shears bands appear only if this feedback is strong enough. If fewer high j orbitals are involved or the low j orbitals are less polarizable, the sequence of the M1 transitions becomes less regular. Also experimentally, the regular shears bands and the irregular

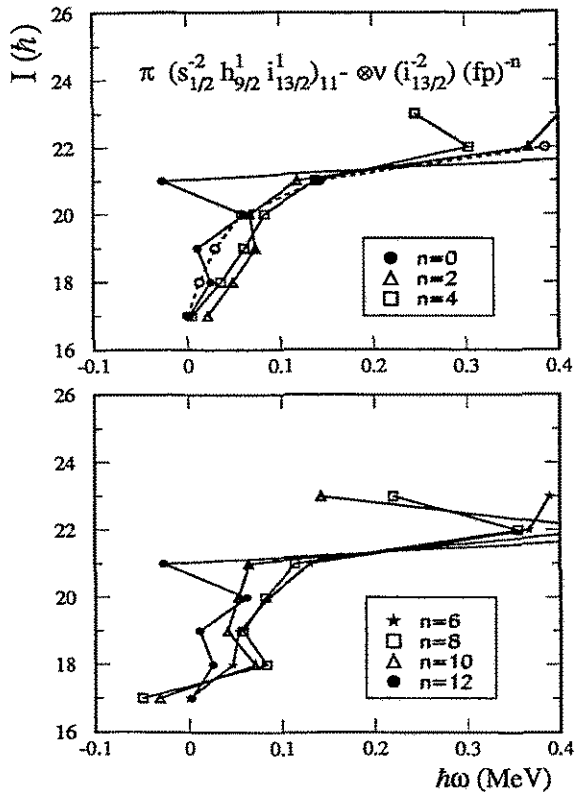


Figure 4: Angular momentum as function of the frequency (transition energy) calculated by means of the shell model. The bands have the configuration $\pi [h_{9/2}, i_{13/2}]_{11}, \pi [s_{1/2}]^{-2}$ and $[\nu i_{13/2}]^{-2}, \nu [fp]^{-n}$.

multiplets are just the two limits of a variety of more or less regular M1 sequences.

The regular M1 sequences with the very weak crossover E2 transitions suggest the concept of *magnetic rotation*. The name accounts for the fact that it is the *magnetic dipole* vector what rotates about the angular momentum vector. In the case of the familiar rotation of well deformed nuclei this role is played by the deformed electrical charge distribution. Thus in this context, the name *electrical rotation* seems to be appropriate for it. The analogies and differences of the two types of rotation are listed in the table. Magnetic rotation extends our concept of collective rotation, emphasizing the fact that it is not always the spatial density distribution that defines the orientation.

Magnetic and electric rotation appear often combined, like e. g. in many high K bands of well deformed nuclei. The new aspect is that there are cases when the electrical part is strongly suppressed or almost absent. Fig. 5 gives an overview where such situations may be expected. The shears bands in the light Pb isotopes and their neighbors are examples of rather pure magnetic rotation. Many regular $\Delta I = 1$ sequences with high BM1 values are also found around $Z = 60$ and $N = 70$. There, the electric part is stronger, since one is further in the open shell where the deformation is larger. It would be interesting to study the nuclei closer to $Z = 50$ and $N = 82$, where a smaller electrical component is expected.

Electric and Magnetic Rotation

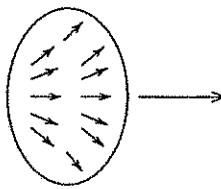
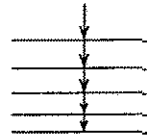
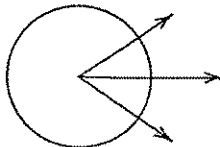
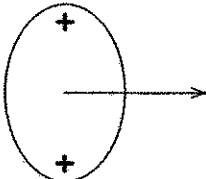
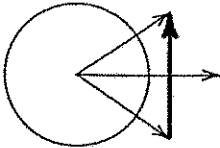
$\Delta I = 2$ ordinary bands	Characteristic of rotational bands	$\Delta I = 1$ shears bands
 <p>gradual alignment of many short vectors</p>	<p>regular $E_\gamma \propto I$</p>  <p>enhanced transitions</p>	 <p>gradual alignment of few long vectors</p>
<p>E2</p>  <p>electric quadrupole mass distribution</p> <p>classic and quantal</p>	<p>possibility to define the orientation (with respect to the a. m. vector)</p> <p>large, collective isotropy broken</p> <p>"inertia" $\mathcal{J}^{(2)} = \Delta I / \Delta E_\gamma$</p>	<p>M1</p>  <p>magnetic dipole current distribution</p> <p>quantal</p>
electric	rotation	magnetic

Table 1: The relation between electric and magnetic rotation

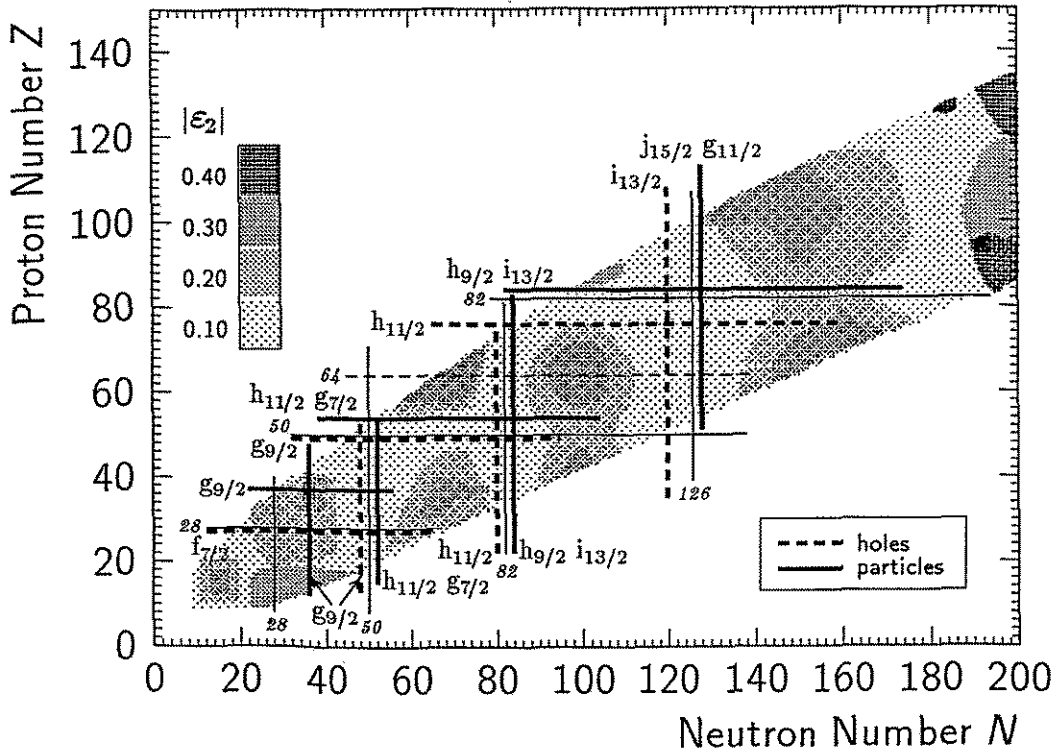


Figure 5: Appearance of magnetic rotation. Full drawn lines indicate the location of the high j particles and dashed ones of the high j holes. The grey scale gives the deformation. The corners where full and dashed lines intersect are particularly favorable for magnetic rotation.

Weakly deformed nuclei may show regular rotational sequences. These are not related to deformed configurations coexisting with the spherical ones. They are a manifestation the rotation of a long magnetic dipole vector, which breaks the spatial isotropy. The finger print of this magnetic rotation are bands with strong M1 and very weak E2 crossover transitions.

3 $\Delta I = 4$ staggering

It has recently been found that some superdeformed $\Delta I = 2$ bands in the mass 150 and 190 regions [8, 9] but also normally deformed nuclei [10, 11] show a slight $\Delta I = 4$ staggering, i. e. the curve found by interpolating the sequence $I = I_0 + 4n$ is by a few keV displaced from the curve obtained by interpolating the sequence $I = I_0 + 2 + 4n$. This energy displacement has been interpreted as a consequence of an inherent fourfold symmetry. The subject is discussed in the lectures by I. Hamamoto, B. Mottelson and I. Pavlichenko [12, 13]. Hamamoto and Mottelson ascribe the staggering to a nonaxial deformation that makes the *long* axis of the nucleus to a fourfold (C_4) symmetry axis. In their approach the bands are described by the rotational hamiltonian

$$H = A_1 I_1^2 + A I_3^2 + B_1 (I_1^2 - I_2^2)^2, \quad A = A_3 - A_1 = \frac{1}{2} \left(\frac{1}{\mathcal{J}_3} - \frac{1}{\mathcal{J}_1} \right) \quad (7)$$

(We have added the first term that is unimportant for the staggering.) It is found that a sizable staggering appears only if $B_1/A > 10^{-2}$.

As an alternative to Hamamoto's and Mottelson's explanation of the origin of the staggering we trace it back to the restriction of the basis in a bandmixing picture (c. f. also the poster by A. Macchiavelli et al. at this conference [14]). Using the conjugate variables I_3 and ϕ , where ϕ is the angle appearing for \vec{I} in polar coordinates, the hamiltonian (7) is given by (c. f. [12])

$$H = A_1 I^2 + A I_3^2 + B_1 I^4 (\cos 2\phi)^2 \quad (8)$$

In the basis $|K\rangle$ of the eigenfunctions of I_3 one has

$$\langle K | (\cos 2\phi)^2 | K' \rangle = -\frac{1}{4} \delta_{KK' \pm 4} + \frac{1}{2} \delta_{KK'} \approx -\frac{d^2}{dK^2} \quad (9)$$

As a consequence of the C_4 symmetry, the hamiltonian couples K only in steps of 4. The eigenvalue problem corresponds to a harmonic oscillator with the spring constant $C = 2A$ and the mass parameter $M = (2I^4 B_1)^{-1}$. The ground state probability distribution has the width $\Delta K = I(B_1/A)^{1/4}$. There is the additional constraint that $K \leq I$. The fact that all components with $K > I$ must be equal to zero makes the yrast energy somewhat larger than the one of the oscillator without the constraint. The constraint is relaxed with increasing I but only in steps of 4, since the K values differ by 4. The $\Delta I = 4$ staggering reflects the fact that every 4 units in I there is a relaxation giving rise to an extra energy gain. However, sizable staggering appears only, if the wavefunction is large enough for $K = I$ to experience the constraint. The numerical calculations indicate that this is the case for $\Psi(K = I)^2 > 5 \times 10^{-5}$ or $B_1/A > 10^{-2}$. From the uncertainty principle it follows that the distribution in ϕ must be sufficiently narrow ($\Delta\phi \sim 1/\Delta K$). This localization requires a sufficiently strong ϕ -dependence of H .

We have used TAC to investigate whether a deformation of the C_4 type is able to generate staggering. Our approach is the following: As any Cranking theory, TAC only permits to calculate the classical energy. This function $E(I, \vartheta, \phi)$ is compared with the energy obtained from the rotational hamiltonian (7) by substituting for the angular momentum operator \vec{I} the classical vector \vec{J} . In other words, the rotational hamiltonian is constructed by quantizing the classical one calculated by means of TAC.

We find the single particle states generated by the TAC routhian

$$h' = h_{mho}(\varepsilon_2) - \hbar\omega_0 \varepsilon_4 \rho^2 (Y_{44} + Y_{4-4}) - \vec{\omega} \cdot \vec{j} \quad (10)$$

$$\vec{\omega} = \omega (\sin \vartheta \cos \phi, \sin \vartheta \sin \phi, \cos \vartheta) \quad (11)$$

as functions of the orientation of the angular velocity, where $h_{mho}(\varepsilon_2)$ is the standard Nilsson hamiltonian. The classical energy is calculated as

$$E(I, \vartheta, \phi) = \langle h' \rangle + \vec{\omega} \cdot \vec{J} \quad (12)$$

where $\vec{J} = \langle \vec{j} \rangle$ and ω is chosen such that $J = I + 1/2$.

As an example, we study $Z = 80$ and $N = 114$ with the deformations $\varepsilon_2 = 0.42$ and $\varepsilon_4 = 0.1$ at the angular momentum $J = 39$ corresponding to $\omega \approx 0.3 MeV$. The deformed potential substantially deviates from axial symmetry. Its shape looks like of a double pyramid with rounded edges.

As seen from eq. (8), the fourth order term disappears for $\phi = 45^\circ$ and the angular momentum components should be given by the relation

$$J_1 = J_1 \omega \sin \vartheta \quad J_3 = J_3 \omega \cos \vartheta \quad (13)$$

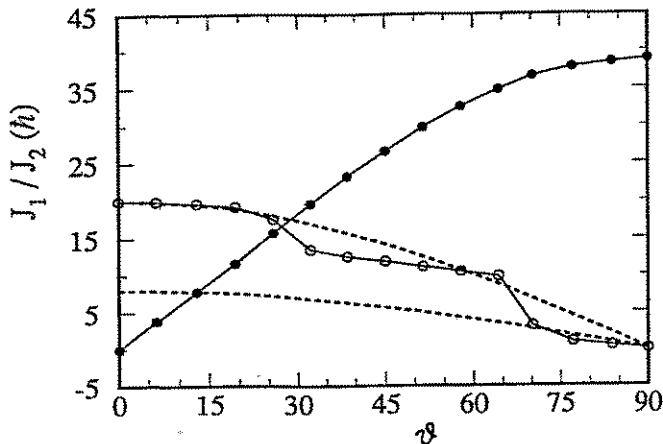


Figure 6: Angular momentum expectation values as functions of the orientation angle ϑ . The filled circles give J_1 and the open circles J_3 .

fixing the two moments of inertia. Fig. 6 shows the calculated angular momenta. The component along the short axis shows the expected dependence, where $\mathcal{J}_1 = 0.13 \text{ keV}^{-1}$. The function $J_3(\vartheta)$ shows steps, indicating rearrangements of particles. Hence, even with the assumed large ε_{44} value the long axis is not very collective and the application of a pure rotor hamiltonian at such high angular momentum is problematic. Accordingly, the determination of \mathcal{J}_3 becomes to certain extent ambiguous. We find $\mathcal{J}_3 = 0.07 \text{ keV}^{-1}$ if we decide to follow the steps adiabatically or $\mathcal{J}_3 = 0.02 \text{ keV}^{-1}$ if the configuration at $\vartheta = 90^\circ$ is kept fixed (c. f. the dashed lines in fig. 6). Hence, our calculations place A in the interval $4 \text{ keV} < A < 21 \text{ keV}$.

The function $E(J, \vartheta = 90^\circ, \phi)$ follows the expected $(\cos(2\phi))^2$ dependence to a good approximation. For the coefficient we find $B_1 J^4 = 50 \text{ keV}$ and 370 keV for the yrast and the lowest neutron p - h excitation, which correspond to $B_1 = 2 \times 10^{-5} \text{ keV}$ and $1 \times 10^{-4} \text{ keV}$, respectively. Even if the lower limit $A = 7 \text{ keV}$ is assumed the ratio $B_1/A \sim 10^{-4} \dots 10^{-5}$. This is much too small to generate any sizable staggering. In order to localize ϕ sufficiently one needs $B_1 > 10^{-2} \times A$, corresponding to the coefficient $B_1 J^4 > 180 \text{ MeV}$ for $J = 40$. It seems hard to imagine how a deformed potential could be capable of producing such a high barrier between the four minima of $E(\phi)$.

Assuming a substantial C_4 distortion for superdeformed ^{194}Hg we are able to construct a classical hamiltonian that has the form of the rotational hamiltonian used by Hamamoto and Mottelson to describe the $\Delta I = 4$ staggering. However, the calculated variation of the energy when turning the angular momentum vector around the C_4 axis is by far too small to allow the quantized version of this hamiltonian to generate a staggering of the observed order of magnitude.

References

- [1] S. Frauendorf, Nucl. Phys. A557 (1993) 259c
- [2] S. Frauendorf, T. Bengtsson, AIP Conference Proceedings 259 (1992) 223

- [3] A. Brokstedt et al. Nucl. Phys. **A571** (1994) 337 and G. Hagemann, lecture at this conference
- [4] G. Baldsiefen et al. Nucl. Phys. **A574** (1994) 521
- [5] J. B. Oliviera et al. Phys. Rev. **D** in print
- [6] H. Hübel, lecture at this conference
- [7] R. M. Clark, lecture at this conference
- [8] S. Flibotte et al., Phys. Rev. Lett. **71** (1993) 4299
- [9] B. Cederwall et al., Phys. Rev. Lett. **72** (1994) 3150
- [10] J. Hamilton, lecture at this conference
- [11] L. Peker et al., Phys. Rev. Lett. **50** (1983) 1749
- [12] I. Hamamoto and B. Mottelson, lectures at this conference
- [13] I. Pavlichenko, lecture at this conference
- [14] A. Macchiavelli et al., contribution to this conference and to be pub.